Kinetic and Spectroscopic Characterization of Intermediates and Component Interactions in Reactions of Methane Monooxygenase from *Methylococcus capsulatus* (Bath)

Katherine E. Liu,[†] Ann M. Valentine,[†] Danli Wang,[‡] Boi Hanh Huynh,*[,‡] Dale E. Edmondson,[§] Athanasios Salifoglou,[†] and Stephen J. Lippard*[,†]

Contribution from the Department of Chemistry, Massachusetts Institute of Technology, Cambridge, Massachusetts 02139, and the Departments of Physics and Biochemistry, Emory University, Atlanta, Georgia 30322

Received June 6, 1995[⊗]

Abstract: We describe mechanistic studies of the soluble methane monooxygenase (sMMO) enzyme system from *Methylococcus capsulatus* (Bath). Interactions among the three sMMO components, the hydroxylase (H), reductase (R), and protein B (B), were investigated by monitoring conversion of nitrobenzene to nitrophenol under both single turnover and catalytic conditions. During catalytic turnover, hydroxylation occurs to afford 3-nitrophenol (43%) and 4-nitrophenol (57%), whereas hydroxylation takes place exclusively (>95%) to give 4-nitrophenol under single turnover conditions in the absence of reductase. Protein B exerts a strong influence on single turnover reactions of nitrobenzene, with optimal rate constants and yields obtained by using 1.5−2 equiv of protein B per equivalent of hydroxylase. The reaction of H_{red} and protein B with dioxygen in the absence of substrate was investigated by using stopped-flow and freeze-quench methodology. In Mössbauer experiments, two distinct populations of diiron sites in H_{red} were detected which react with dioxygen on different time scales. Deconvolution of the time-dependent Mössbauer spectra allowed the isomer shift (δ) and quadrupole splitting (ΔE_Q) parameters as well as the kinetic constants to be extracted for each species. For the faster reacting, physiologically relevant component $H_{red}(1)$, two kinetically competent intermediates were identified. The first intermediate, H_{peroxo} (δ = 0.66 mm/s; ΔE_Q = 1.51 mm/s), a diiron(III) peroxide species, forms with a rate constant of $\approx$25 s^{-1} and decays with a rate constant of $\approx$0.45 s^{-1} at 4 °C. Rate constants for the formation and decay of the second intermediate, Q, which absorbs with $\lambda_{max} \approx 350$ and 420 nm and can also be followed by kinetic freeze-quench Mössbauer spectroscopy (δ = 0.21 mm/s; ΔE_Q = 0.68 mm/s and δ = 0.14 mm/s; ΔE_Q = 0.55 mm/s), are $k_{form} \approx 0.45$ s^{-1} and $k_{decay} \approx 0.05$ s^{-1} at 4 °C. The temperature dependence of these kinetic values was determined. Changes in dioxygen concentration and pH, as well as exchange of solvent accessible protons with D_2O, did not significantly affect the rate constants for either of these processes, the implications of which for the kinetic mechanism are discussed. From the present and related evidence, structures for H_{peroxo} and Q are proposed.

Introduction

Methane monooxygenase (MMO) converts methane into methanol in the first step in the metabolic pathway of methanotrophs (eq 1).[1] MMO exists in both a particulate, membrane-

$$CH_4 + O_2 + H^+ + NADH \rightarrow CH_3OH + H_2O + NAD^+ \quad (1)$$

bound form containing copper and a soluble form containing iron at the active site.[2] Soluble methane monooxygenase (sMMO) isolated from *Methylococcus capsulatus* (Bath) and *Methylosinus trichosporium* OB3b, two of the better characterized systems, comprises three separate proteins, a hydroxylase (H), protein B, and a reductase (R).[3]

The hydroxylase component of sMMO is a member of the protein family containing carboxylate-bridged dinuclear iron units[4] at their active sites. Included are hemerythrin, the R2 subunit of ribonucleotide reductase, rubrerythrin, the ferroxidase center of ferritin, and purple acid phosphatase.[5−7] We wish to understand the factors responsible for tuning the diiron centers in these proteins to perform their specific functions, which range from the reversible binding of dioxygen in hemerythrin to its activation for the hydroxylation of methane in sMMO. In pursuit of this objective, we are investigating the proteins of the sMMO system and exploring the fundamental chemistry of the diiron center in the hydroxylase.

As isolated, the hydroxylase contains up to two dinuclear iron centers in the oxidized $Fe^{III}Fe^{III}$ (H_{ox}) form,[8] which provide sites for substrate binding and activation. The mixed-valent Fe^{II}-Fe^{III} (H_{mv})[9] and fully reduced $Fe^{II}Fe^{II}$ (H_{red}) redox states are readily accessible through chemical reduction of H_{ox}. The crystal structure of H_{ox} from *M. capsulatus* (Bath)[10] revealed the Fe atoms to be bridged by a hydroxide ion and a bidentate, semibridging glutamate ligand. Each metal is also coordinated to a histidine ligand. Two additional glutamate residues ligate

[†] Massachusetts Institute of Technology.
[‡] Department of Physics, Emory University.
[§] Department of Biochemistry, Emory University.
[⊗] Abstract published in *Advance ACS Abstracts,* October 1, 1995.

(1) Anthony, C. *The Biochemistry of Methylotrophs*; Academic Press: New York, 1982; pp 296−379.
(2) Stanley, S. H.; Prior, S. D.; Leak, D. J.; Dalton, H. *Biotech. Lett.* **1983**, *5*, 487−492.
(3) (a) Lipscomb, J. D. *Annu. Rev. Microbiol.* **1994**, *48*, 371−399. (b) Liu, K. E.; Lippard, S. J. *Adv. Inorg. Chem.* In press.
(4) Feig, A. L.; Lippard, S. J. *Chem. Rev.* **1994**, *94*, 759−805.
(5) Que, L., Jr.; True, A. E. *Prog. Inorg. Chem.* **1990**, *38*, 97−200.
(6) Kurtz, D. M. *Chem. Rev.* **1990**, *90*, 585−606.
(7) Wilkins, R. G. *Chem. Soc. Rev.* **1992**, 171−178.
(8) Fox, B. G.; Lipscomb, J. D. *Biochem. Biophys. Res. Commun.* **1988**, *154*, 165−170.
(9) Woodland, M. P.; Patil, D. S.; Cammack, R.; Dalton, H. *Biochim. Biophys. Acta* **1986**, *873*, 237−242.

0002-7863/95/1517-10174$09.00/0

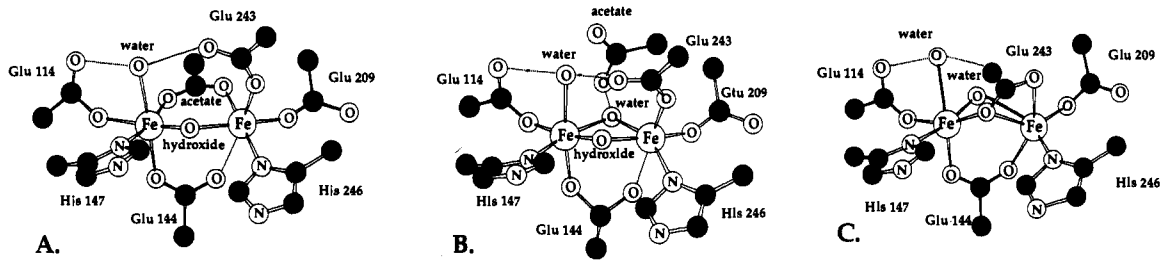

Figure 1. Active site structures of sMMO hydroxylase from *M. capsulatus* (Bath). (A) H_{ox} at 4 °C and 2.2 Å resolution. (B) H_{ox} in flash-frozen crystals at 1.7 Å resolution and −160 °C. Note that an exogenous ligand, tentatively assigned as acetate, in (A) has been replaced by a coordinated water molecule to which it is now hydrogen bonded. (C) H_{red} obtained by soaking crystals of H_{ox} in sodium dithionite and methyl viologen. Crystals were flash-frozen at −160 °C. In all three drawings, short dashed lines indicate hydrogen bonding and long dashed lines indicate little to no coordination.

one Fe atom in a monodentate fashion, whereas the other has a monodentate glutamate and a water molecule in its coordination sphere. Finally, octahedral coordination at each of the iron atoms is completed by an exogenous bridging ligand, assigned either as water or, tentatively, acetate from the crystallization buffer, depending upon the conditions used to prepare crystals for X-ray diffraction experiments (Figure 1, A and B).[10] In the reduced protein, H_{red},[10b] a carboxylate shift and loss of the bridging hydroxide and the water or acetate ligand afford the structure shown in Figure 1C. Other physical techniques,[11-16] including EXAFS, EPR, ENDOR, MCD, and Mössbauer spectroscopy, have supported these assignments for the iron coordination environment in sMMO from both *M. capsulatus* (Bath) and *M. trichosporium* OB3b.

During catalysis (eq 1), the reductase accepts electrons from NADH and transfers them to the dinuclear iron centers in the hydroxylase.[17-19] H_{red}, the species reactive toward dioxygen, can also be produced by chemical reduction of H_{ox} with sodium dithionite in the presence of mediators. Protein B from *M. capsulatus* (Bath) may regulate electron transfer from the reductase to the hydroxylase.[20,21] The effects of protein B in the *M. trichosporium* OB3b sMMO system include its ability to lower the reduction potential of the hydroxylase,[22] perturb the EPR signal of H_{mv},[23] alter product distributions of the hydroxylation reaction,[24,25] and change the initial velocity of the completely reconstituted system.[25] Little is known about the influence of the reductase and protein B on the reaction chemistry of the hydroxylase. Further examination of interactions among the three components, which influence their collective behavior in the sMMO system, is necessary to elucidate fully the role of each protein in catalysis.

The present investigation was undertaken initially to explore the effects of the reductase and protein B components on the kinetic constants, regioselectivity, and product yields of the reaction of H_{red} with nitrobenzene and dioxygen. The substrate nitrobenzene produces highly colored products upon oxidation.[24,25] Since neither H_{red} nor H_{ox} has any absorption bands above 300 nm, this reaction is readily followed by optical spectroscopy. In the course of these studies, spectral changes were detected in a control reaction of H_{red} with dioxygen even in the absence of substrate. Kinetic constants for the formation and decay of these colored species were therefore determined, leading to their assignment as intermediates along the reaction pathway. Spectroscopic and kinetic characterization of these intermediates was obtained by using stopped-flow spectrophotometry and rapid freeze-quench EPR, Mössbauer, and resonance Raman spectroscopy. In the present article we describe our findings in the above areas, some aspects of which were communicated previously,[26,27] and suggest assignments for intermediates in a proposed catalytic reaction cycle. Parallel studies with sMMO from *M. trichosporium* OB3b were reported while our work was in progress.[28,29]

Experimental Section

Bacterial Growth and Protein Purification. Growth of the native *M. capsulatus* (Bath) organism and purification of the hydroxylase, protein B, and reductase components of its sMMO were performed as described elsewhere.[14,30] Specific activities and iron contents were in the ranges reported.[30] Hydroxylase activities of up to 600 mU/mg were obtained with an assay system consisting of purified H_{ox}, protein B, and reductase with propylene as the substrate. For Mössbauer work, H_{ox} enriched with ^{57}Fe was obtained from cells grown on the usual medium[31] except that $Na^{57}FeEDTA$ was added as the sole source of iron. $Na^{57}FeEDTA$ was prepared by dissolving ^{57}Fe foil (52 mg, 0.91 mmol, 95% enriched, Cambridge Isotope Labs) in 3.6 mL of 1 M ultrapure HNO_3. Next, 3.6 mL of H_2O and 0.58 g (2 mmol) of Na_2-EDTA·$2H_2O$ were added. After the solution was stirred for 5 min, 30 mg (0.75 mmol) of NaOH was added to the iron solution. The resulting

(10) (a) Rosenzweig, A. C.; Frederick, C. A.; Lippard, S. J.; Nordlund, P. *Nature* **1993**, *366*, 537-543. (b) Rosenzweig, A. C.; Nordlund, P.; Takahara, P. M.; Frederick, C. A.; Lippard, S. J. *Chem. Biol.* **1995**, 2, 409-418.

(11) Fox, B. G.; Hendrich, M. P.; Surerus, K. K.; Andersson, K. K.; Froland, W. A.; Lipscomb, J. D.; Münck, E. *J. Am. Chem. Soc.* **1993**, *115*, 3688-3701.

(12) DeRose, V. J.; Liu, K. E.; Kurtz, D. M., Jr.; Hoffman, B. M.; Lippard, S. J. *J. Am. Chem. Soc.* **1993**, *115*, 6440-6441.

(13) Hendrich, M. P.; Fox, B. G.; Andersson, K. K.; Debrunner, P. G.; Lipscomb, J. D. *J. Biol. Chem.* **1992**, *267*, 261-269.

(14) DeWitt, J. G.; Bentsen, J. G.; Rosenzweig, A. C.; Hedman, B.; Green, J.; Pilkington, S.; Papaefthymiou, G. C.; Dalton, H.; Hodgson, K. O.; Lippard, S. J. *J. Am. Chem. Soc.* **1991**, *113*, 9219-9235.

(15) DeRose, V. J.; Liu, K. E.; Lippard, S. J.; Hoffman, B. M. Submitted for publication.

(16) Bender, C. J.; Rosenzweig, A. C.; Lippard, S. J.; Peisach, J. *J. Biol. Chem.* **1994**, *269*, 15993-15998.

(17) Lund, J.; Dalton, H. *Eur. J. Biochem.* **1985**, *147*, 291-296.

(18) Lund, J.; Woodland, M. P.; Dalton, H. *Eur. J. Biochem.* **1985**, *147*, 297-305.

(19) Green, J.; Dalton, H. *Biochem. J.* **1989**, *259*, 167-172.

(20) Green, J.; Dalton, H. *J. Biol. Chem.* **1985**, *260*, 15795-15801.

(21) Liu, K. E.; Lippard, S. J. *J. Biol. Chem.* **1991**, *266*, 12836-12839.

(22) Paulsen, K. E.; Liu, Y.; Fox, B. G.; Lipscomb, J. D.; Münck, E.; Stankovich, M. T. *Biochemistry* **1994**, *33*, 713-722.

(23) Fox, B. G.; Liu, Y.; Dege, J. E.; Lipscomb, J. D. *J. Biol. Chem.* **1991**, *266*, 540-550.

(24) Andersson, K. K.; Froland, W. A.; Lee, S.-K.; Lipscomb, J. D. *New J. Chem.* **1991**, *15*, 411-415.

(25) Froland, W. A.; Andersson, K. K.; Lee, S.-K.; Liu, Y.; Lipscomb, J. D. *J. Biol. Chem.* **1992**, *267*, 17588-17597.

(26) Liu, K. E.; Wang, D.; Huynh, B. H.; Edmondson, D. E.; Salifoglou, A.; Lippard, S. J. *J. Am. Chem. Soc.* **1994**, *116*, 7465-7466.

(27) Liu, K. E.; Valentine, A. M.; Qiu, D.; Edmondson, D. E.; Appelman, E.; Spiro, T. G.; Lippard, S. J. *J. Am. Chem. Soc.* **1995**, *117*, 4997-4998.

(28) Lee, S.-K.; Fox, B. G.; Froland, W. A.; Lipscomb, J. D.; Münck, E. *J. Am. Chem. Soc.* **1993**, *115*, 6450-6451.

(29) Lee, S.-K.; Nesheim, J. C.; Lipscomb, J. D. *J. Biol. Chem.* **1993**, *268*, 21569-21577.

(30) Liu, K. E.; Johnson, C. C.; Newcomb, M.; Lippard, S. J. *J. Am. Chem. Soc.* **1993**, *115*, 939-947.

(31) Pilkington, S. J.; Dalton, H. In *Methods In Enzymology*; Academic Press: New York, 1990; Vol. 188, pp 181-190.

mixture was stirred for 6 h, after which time it was centrifuged to pellet the precipitate. The dark green supernatant was added to 100 mL of 20 mM sodium phosphate buffer (pH 7.0). The resulting solution was added to the normal growth medium to a final iron concentration of 36 μM. Specific activities and iron content of ^{57}Fe enriched hydroxylase were as reported for native hydroxylase.

Generation of H_{red}. To reduce the hydroxylase, a stoichiometric amount of a 10 mM solution of methyl viologen was added to H_{ox} as an electron transfer mediator. The protein and mediator solution was then made anaerobic by evacuation and back-filling with argon for at least 5 cycles. Next, a 0.1 M solution of sodium dithionite was prepared by first degassing 2 mL of buffer (25 mM MOPS, pH 8.5) for 15 min with dioxygen-free argon. Degassed buffer was transferred with a gastight syringe to a vial which contained 41 mg (0.23 mmol) of sodium dithionite, previously made anaerobic by evacuation and back-filling with argon for 3 cycles. An aliquot of the sodium dithionite solution was then added to the protein solution by means of a gastight syringe to achieve a 2-fold molar excess concentration over that of the hydroxylase. Upon addition of the reductant, the reaction mixture immediately turned blue due to formation of the methyl viologen radical. Reduction was allowed to proceed for at least 45 min, during which time the reaction mixture was transferred to an anaerobic chamber. Inside this glovebox the protein solution was placed into dialysis tubing having a 10 000 molecular weight cutoff and then dialyzed for 2 h against 400 mL of 25 mM MOPS, pH 7.0 buffer to remove methyl viologen and excess sodium dithionite.

Experiments with protein B and reductase were performed in two different ways. Reduction of H_{ox} to H_{red} was first carried out, after which the other component(s) was added to the dialyzed protein. Alternatively, the additional component(s) was combined with H_{ox} prior to reduction, with subsequent treatments as described.

Single Turnover Reactions. Kinetic Studies. The reduced, dialyzed protein solution was diluted with 25 mM MOPS, pH 7.0 buffer to achieve a 50 μM concentration of H_{red}. Protein B concentrations ranged from 0 to 200 μM. The substrate nitrobenzene was added as the neat liquid, 10 μL per 1 mL of protein solution, to obtain saturation at approximately 5 mM. The resulting mixture was incubated for 5 min, after which time undissolved nitrobenzene was removed by pipet. For stopped-flow kinetic analysis, the protein mixture was loaded into a 10 mL Hamilton gastight syringe and then removed from the glovebox (vide infra). The reaction was initiated by mixing with dioxygen-saturated buffer, and optical changes at 404 nm were recorded to monitor the formation of 4-nitrophenol.

Product Distribution and Yields. To determine the distribution of products from nitrobenzene hydroxylation, enzymatic reactions were typically performed with 8 mg (3.2×10^{-8} mol) of hydroxylase and variable quantities of protein B and reductase. Up to 2.2 mg (1.3×10^{-7} mol) of protein B and 5 mg (1.3×10^{-7} mol) of reductase were added to achieve ratios from 0 to 4 equiv for a given component relative to the hydroxylase. The reaction mixture was reduced, dialyzed, and incubated with substrate as outlined above. After dialysis, the mixture ($\approx$1 mL) was transferred to a 10 mL glass vial which was then sealed with a septum. The vial was brought out of the box, and 0.5 mL of dioxygen-saturated buffer was injected by syringe through the septum. The resulting solution was placed in a shaking incubator maintained at 45 °C and allowed to react for at least 15 min to ensure completion of the reaction. To compare the regioselectivity of the catalytic system to that obtained in single turnover reactions, 1.5 mg (6×10^{-9} mol) of hydroxylase, 0.2 mg (1.2×10^{-8} mol) of protein B, 0.4 mg (1.2×10^{-8} mol) of reductase, and 1 μL (8×10^{-6} mol) of nitrobenzene were combined in a total volume of 0.5 mL. This mixture was incubated for 30 s at 45 °C in a capped vial. By means of a syringe, 25 μL of a 0.1 M ethanol-free solution of NADH was then added through the septum and the mixture was allowed to react for 15 min at 45 °C.

The distribution of 2-, 3-, and 4-nitrophenol products formed in enzymatic reactions with nitrobenzene was investigated through HPLC analysis. The reaction mixtures were treated with 200 μL of a 3% trichloroacetic acid solution to precipitate the protein. The resulting suspension was centrifuged for 2 min in a table top centrifuge to pellet the protein. An aliquot from the supernatant was then injected into the HPLC, and the identities of the reaction components were determined by comparison of their retention times with those of authentic standards of the expected products. Further details are available as supporting information.

The overall yields of products formed in a single turnover reaction of H_{red} with nitrobenzene were calculated by first determining the amount of 4-nitrophenol that was generated. The corresponding amounts of 2- and 3-nitrophenol for the appropriate ratio of protein B to hydroxylase as determined by the above HPLC analysis were next added to this value to determine the total product formed. Finally, the amount of product was divided by the number of dinuclear iron centers present in the reaction solution to determine the percent yield of the reaction.

To optimize the yield of 4-nitrophenol in single turnover reactions, several conditions were investigated and their effects were compared. The incubation time to reduce H_{ox} was varied from 30 min to 2 h. Reactions with variable quantities of protein B were performed. Reductase alone and a mixture of both protein B and reductase were added to the hydroxylase in parallel reactions. Nitrobenzene was also added prior to the addition of sodium dithionite to determine whether the order of addition of reductant and substrate affected the yield of this product.

Stopped-Flow Spectrophotometry. Stopped-flow experiments were performed to monitor the reaction of H_{red} with dioxygen in the presence of 2 equiv of protein B. This ratio of components was chosen because it gave optimal rate constants and yields from single turnover reactions with nitrobenzene (vide infra). Dialyzed solutions of H_{red} (typically 60 to 200 μM) and protein B were loaded into a 10 mL Hamilton gastight syringe fitted with a KelF threaded adapter for connection to an anaerobic line of a stopped-flow assembly (HiTech, Canterbury, England). The contents of the 10 mL syringe were used to fill the drive syringe of the stopped-flow apparatus. By using a Matheson gas mixer, buffer (25 mM MOPS, pH 7.0) with variable concentrations of dioxygen (0 to 1 mM) was prepared and then loaded into the second drive syringe of the stopped-flow assembly. Solutions were equilibrated for 30 min at a given temperature prior to mixing. To determine the pH dependence of the reaction of H_{red} with dioxygen, the anaerobic dialysis was performed with 400 mL of 10 mM MOPS, pH 7.0. The oxygenated buffer solution contained 100 mM MOPS buffer, with pH values ranging from 6.6 to 8.6. To test for the presence of a deuterium isotope effect on the reaction velocities, hydroxylase was first exchanged into D_2O by using a procedure described elsewhere.[12] A small volume ($\approx$175 μL) of a 5 mM solution of protein B was added to the exchanged H_{ox} (2 mL) prior to reduction. A stock solution of 25 mM MOPS in D_2O was used to make the 0.1 M sodium dithionite solution (pD = 8.5, uncorrected for the deuterium isotope effect) for the dialysis and as the oxygenated buffer in the second drive syringe (pD = 7.0, uncorrected).

For reactions with the substrates hexane and methane, the oxygenated buffer was further treated as follows. With hexane, 100 mL of dioxygen-saturated 25 mM MOPS, pH 7.0 buffer was mixed with 50 mL of hexane for 20 min to obtain a saturated solution of this substrate. The aqueous layer was removed and used to fill the aerobic drive syringe. With methane, a similar procedure was used, except that 25 mL of dioxygen-saturated buffer was incubated with 25 mL of methane gas at approximately atmospheric pressure.

Spectrophotometric analysis was performed with one of two detection systems. A photomultiplier tube was used to collect data at single wavelengths between 330 and 800 nm. Alternatively, a Hewlett Packard UV/vis diode array spectrophotometer (model 8452A) was used to collect data at multiple wavelengths.

Rapid Freeze-Quench Mössbauer Spectroscopic Studies. Mössbauer samples were made with ^{57}Fe-enriched hydroxylase. Freeze-quench studies were performed with an Update Instruments rapid freeze-quench apparatus following methods outlined elsewhere.[32] Solutions of 600–700 μM H_{red} and 1.2–1.4 mM protein B were mixed rapidly with a dioxygen-saturated ($\approx$1 mM) 25 mM MOPS, pH 7.0 buffer solution at 4 °C. Protein was allowed to react with dioxygen for fixed time periods (0.025–60 s) before being sprayed into isopentane at −140 °C.

Mössbauer spectra were collected by using either a weak-field spectrometer equipped with a Janis 8DT variable-temperature cryostat

(32) Ravi, N.; Bollinger, J. M., Jr.; Huynh, B. H.; Edmondson, D.; Stubbe, J. *J. Am. Chem. Soc.* **1994**, *116*, 8007–8014.

Table 1. Product Distributions (%) from Reactions of MMO with Nitrobenzene[a]

organism	components	reductant	4-nitrophenol	3-nitrophenol
M. capsulatus (Bath)	$H_{ox} \pm B$	chemical[b]	>95	
	H_{ox}, B, R	NADH	57	43
M. trichosporium OB3b[c]	H_{ox}, B, R	NADH	89	11
	H_{ox}, R	NADH	<10	>90
	H_{ox}	H_2O_2	38	59
	H_{ox}, B	H_2O_2	59	41

[a] In all cases, very little 2-nitrophenol was detected. [b] H_{ox} was reduced with sodium dithionite in the presence of methyl viologen as described in the Experimental Section. [c] References 24 and 25.

or a strong-field spectrometer outfitted with a Janis 12 CNDT/SC SuperVaritemp cryostat encasing an 8 T superconducting magnet. A constant acceleration mode in a transmission geometry was used to operate both spectrometers. The centroid of the room temperature spectrum of a metallic iron foil corresponds to the zero velocity of the Mössbauer spectra.

Results

Studies of Nitrobenzene Hydroxylation. Product Distribution and Yields in Single Turnover Experiments. In single turnover reactions of H_{red} and various ratios of protein B, the predominant product was always 4-nitrophenol. By contrast, under catalytic conditions, in which all components were present and NADH sustained turnover, a mixture of 57% 4-nitrophenol and 43% 3-nitrophenol was produced. Product distributions under the various conditions tested are summarized in Table 1.

Optimal product yields in single turnover studies were obtained with a 45 min incubation time of reductant with H_{ox} and a subsequent 2 h dialysis period. In all cases where an additional component(s) was incubated with the hydroxylase, the results were the same irrespective of whether the protein(s) was added to either H_{ox} or H_{red}. Yields from reactions of H_{red} with nitrobenzene in the presence of reductase were similar to those obtained with H_{red} alone (<10%). Incubation with both protein B and reductase present resulted in low yields, approximately 75% less than with the H_{red} alone. The addition of protein B in the absence of reductase had a dramatic effect on the yield, tripling the absorbance change at 404 nm compared to a reaction with only H_{red} present. Increasing amounts of 4-nitrophenol were detected as the B:H_{red} ratio increased, saturating at 2 equiv of B, where the yield was ≈40%. A plot of the percent yield of product versus the number of equivalents of protein B is given in the supporting information.

Kinetic Analysis of the Hydroxylation of Nitrobenzene. Kinetic traces from single turnover reactions of H_{red} and H_{red} plus protein B were obtained under pseudo-first-order conditions in dioxygen and nitrobenzene (Figure S2). A rate constant was derived from each trace after fitting to the first-order growth equation indicated in eq 2. A plot of k_{obs} values obtained in

$$y = A + m[1 - \exp(-k_{obs}t)] \quad (2)$$

this manner as a function of the B:H ratio is given in Figure 2, from which it is apparent that addition of B increases k_{obs} from 0.011 s^{-1} to a maximum value of 0.40 s^{-1} at a 1.5−2.0:1 B:H molar ratio. Further addition of protein B diminishes k_{obs} slightly, and above 2.5 equiv the rate constant levels off at ≈0.25 s^{-1}. Protein B therefore induces a maximal increase of ≈35-fold in k_{obs}.

Intermediates Formed in the Reaction of H_{red} with Dioxygen. Mössbauer Spectroscopic Characterization of Reaction Components; H_{red}. A zero-field Mössbauer spectrum of H_{red} from *M. capsulatus* (Bath) recorded at 4.2 K is shown

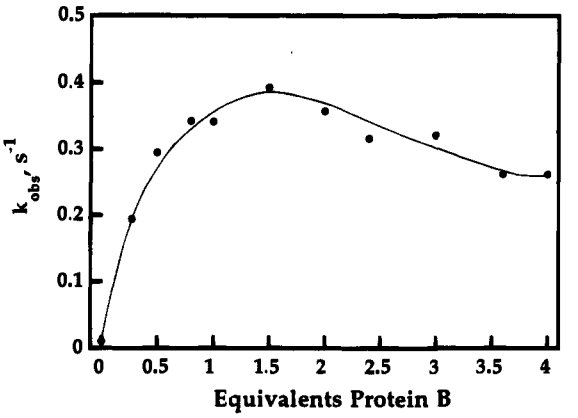

Figure 2. The observed rate constant of product formation, k_{obs}, at 4 °C as a function of protein B concentration.

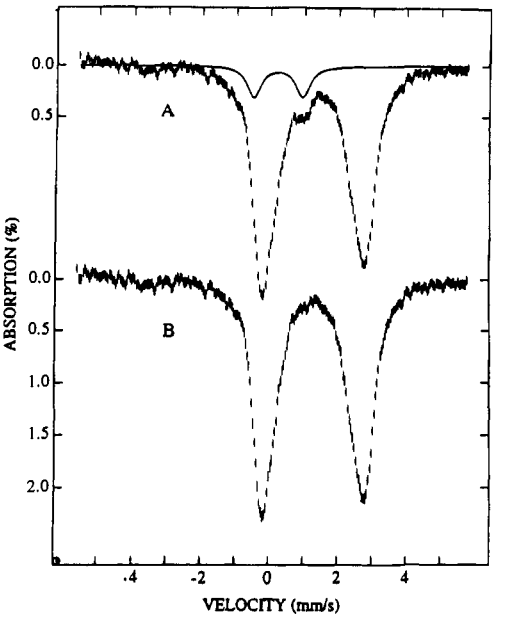

Figure 3. Zero-field Mössbauer spectrum of H_{red} at 4.2 K: (A) the raw data, with the 10% ferric impurity designated by a solid line; (B) the data with that impurity subtracted.

in Figure 3. A major quadrupole doublet with broad absorption lines (line width ≈ 0.8 mm/s) is observed, the measured apparent parameters for which are $\Delta E_Q = 2.87$ mm/s and $\delta = 1.30$ mm/s. These values are characteristic of high-spin ferrous species ($S = 2$) coordinated by oxygen and nitrogen donors, as expected for the reduced diferrous center in H_{red}. The breadth of the peaks could arise either from inequivalent iron sites, inhomogeneity of the protein environment of the dinuclear center, or a combination of the two. The freeze-quench kinetic data presented below indicate that there are at least two diferrous components in H_{red} which are readily discernible by their rates of reaction with dioxygen. These components exhibit spectra that are indistinguishable when recorded in the absence of an applied magnetic field.

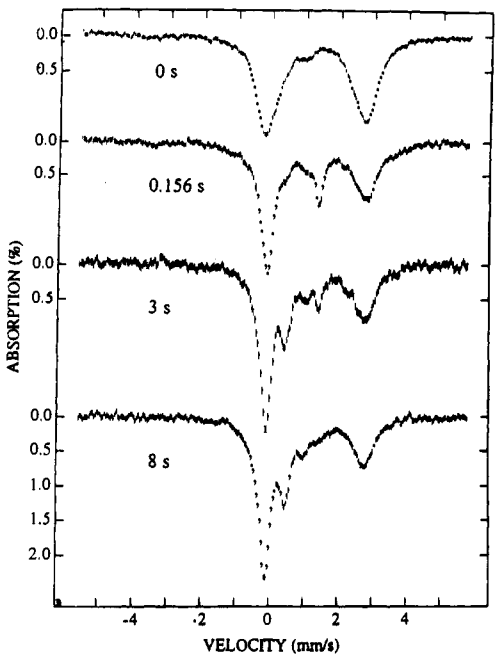

Figure 4. Time-dependent Mössbauer spectra following the interaction of H_{red} with dioxygen at 4°C. The spectra shown correspond to reaction times of 0 s, 156 ms (at which time the amount of H_{peroxo} is maximized), 3 s, and 8 s (at which time the concentration of Q maximizes).

In addition to the major doublet, the spectrum exhibits a shoulder at ≈1 mm/s. This absorption is the high-energy line of a minor quadrupole doublet, the parameters of which are estimated to be $\Delta E_Q = 1.1-1.3$ mm/s and $\delta = 0.3-0.5$ mm/s, typical for high-spin ferric species. This signal (≈10%) was detected in all samples and is assigned as a ferric impurity. A spectrum representing H_{red} can therefore be prepared by removing the 10% contribution of this impurity from the raw data. Such a prepared spectrum (Figure 3) was used in the analysis of the decay of the ferrous components in the reaction of H_{red} with dioxygen.

Decay of the Ferrous Components in H_{red} Following Exposure to Dioxygen. Figure 4 shows the time-dependent Mössbauer spectra of the reaction of H_{red} with dioxygen. Reactions were quenched at 0, 0.156, 3, and 8 s. The data were recorded at 4.2 K in the absence of an applied magnetic field. Under these conditions, the high-energy line at ≈2.8 mm/s of the ferrous components of H_{red} is well resolved from other spectral components. The amount of the ferrous components in each sample could therefore be accurately (±5%) quantitated by using the prepared H_{red} spectrum (Figure 3B) as a reference. Figure 5 shows a plot of the percent absorption of the ferrous components as a function of time after reaction of H_{red} with dioxygen. From this plot, it is evident that there are at least two ferrous components in H_{red} which react with dioxygen at different rates, one fast and one more slowly, and are designated $H_{red}(1)$ and $H_{red}(2)$, respectively. The data were therefore analyzed by assuming two independent exponential decays according to eq 3, where A is the percent absorption of the total

$$A = A^0_1 \exp(-k_1 t) + A^0_2 \exp(-k_2 t) \quad (3)$$

ferrous components and A^0_1 and A^0_2 are the initial percent absorption values for the ferrous components $H_{red}(1)$ and $H_{red}(2)$, respectively. The solid line in Figure 5 is the least-squares fit of the data according to eq 3, where $A^0_1 = 32 \pm 6\%$, $A^0_2 = 57 \pm 10\%$, $k_1 = 24 \pm 5$ s^{-1}, and $k_2 = 0.01 \pm 0.01$ s^{-1}. The decay rate for $H_{red}(2)$ is too slow to be of catalytic significance since the turnover rate is approximately 0.3 s^{-1};[19]

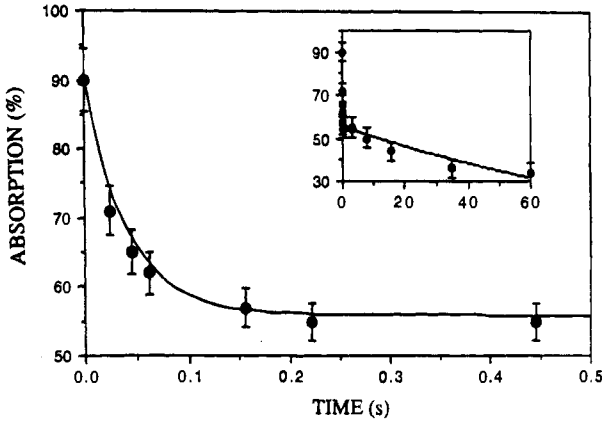

Figure 5. The two-phase disappearance of H_{red} as determined by kinetic Mössbauer experiments at 4 °C, showing the fast decay of $H_{red}(1)$ and the slower decay of $H_{red}(2)$ (inset).

we therefore assign this component as inactive hydroxylase. Additionally, the decay of $H_{red}(1)$ parallels the formation of a reaction intermediate, the diiron(III) peroxo species (vide infra), strongly implying that $H_{red}(1)$ represents active H_{red}.

The data shown in Figure 5 could also be fit with three independent exponential decay processes. Inclusion of an additional decay improved only the fit at longer time points (>8 s) and had no effect on either the initial percentage or the decay rate constant for $H_{red}(1)$. With a decay rate constant of 24 s^{-1} for $H_{red}(1)$, which corresponds to a half-life of 0.03 s, the observed ferrous absorption at reaction times longer than 3 s corresponds mostly to that of $H_{red}(2)$. Careful comparison of the high-energy line of the ferrous absorption of the spectrum obtained when the reaction was quenched at 0 s with that at 8 s in Figure 4 reveals that, within experimental error, the spectra of $H_{red}(1)$ and $H_{red}(2)$ are indistinguishable at zero field. The two components exhibit different magnetic behavior under the influence of strong applied magnetic fields (4–8 T), however, and at long times (>60 s) $H_{red}(1)$ disappears. The many parameters required to analyze the strong-field Mössbauer spectrum, 21 for just a single diferrous center assuming the principal axes for all the hyperfine tensors to be coincident, precludes a unique and more detailed interpretation of the spectra of $H_{red}(1)$ and $H_{red}(2)$.

H_{ox}. The 4.2-K zero-field spectrum of H_{ox} from *M. capsulatus* (Bath) is shown in Figure 6C. This sample was prepared by the reaction of H_{red} with dioxygen. Removal of a 12% ferrous contribution and the 10% ferric impurity results in a spectrum representing H_{ox} (Figure 6B), the partially resolved quadrupole doublets of which clearly demonstrate the presence of more than one iron species in the sample. Since the spectrum is only partially resolved, the following assumption was made in order to reduce the number of variable parameters in the analysis. The spectrum was assumed to originate from two different diferric centers, corresponding to oxidation of the two diferrous components described above. Since each diiron center generates two quadrupole doublets of equal intensity, the spectrum was fit with four quadrupole doublets but only two absorption intensities. The deconvoluted spectral parameters are listed in Table 2. The fitting of the Mössbauer spectrum of $H_{ox}(2)$ resulted in an unusually high value for δ (0.72 mm/s), which we attribute to two or more unresolved species contributing to this signal. Failure to resolve the low velocity component of the quadrupole doublet can lead to an underestimate of ΔE_Q and an artificially high value of δ. This analysis agrees with kinetic behavior of $H_{red}(2)$, since the decay of its Mössbauer signal is best fit with two independent exponentials. The two doublets with smaller ΔE_Q values are assigned to the diferric

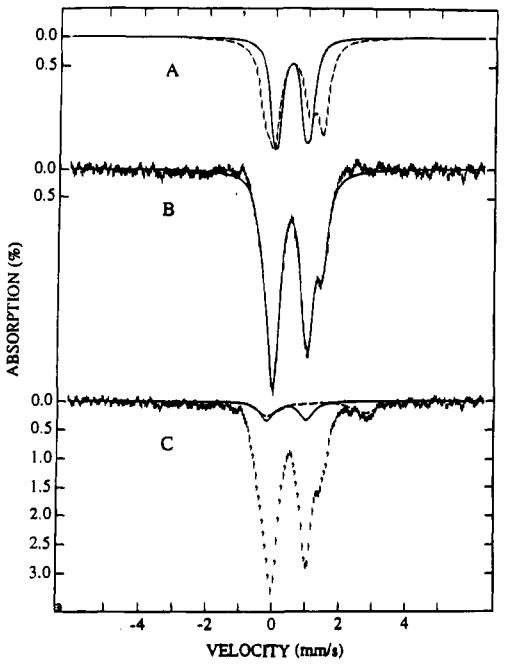

Figure 6. Deconvolution of the Mössbauer signal for H_{ox} revealing several components. Spectrum C shows the raw data along with the contribution from the 10% inactive diferric impurity (solid line) and unreacted H_{red} (dashed line). Spectrum B represents the data with contributions from these sources digitally subtracted. The data are further resolved into $H_{ox}(1)$ (solid line) and $H_{ox}(2)$ (dashed line) in spectrum A.

Table 2. Mössbauer Parameters (4 K) of Species Detected in Rapid Freeze–Quench Samples from the Reaction of H_{red} with Dioxygen

species	$\delta \pm 0.02$ mm/s	$\Delta E_Q \pm 0.03$ mm/s
$H_{ox}(1)$ (site 1)	0.51	1.12
$H_{ox}(1)$ (site 2)	0.50	0.79
$H_{ox}(2)$ (site 1)	0.72	1.46
$H_{ox}(2)$ (site 2)	0.47	1.33
$H_{red}(1)$	1.3	2.8
$H_{red}(2)$	1.3	2.8
H_{peroxo}	0.66	1.51
Q (site 1)	0.21	0.68
Q (site 2)	0.14	0.55

center that arises following fast reaction of $H_{red}(1)$ with dioxygen, termed $H_{ox}(1)$, whereas the other two doublets are assigned to the more slowly reacting diiron center, termed $H_{ox}(2)$. The spectra of these two diferric components are also shown in Figure 6A. These assignments are based mainly on the kinetic studies, which indicate that $H_{ox}(1)$ forms with the same rate constant as that of the decay of the reaction intermediate Q (vide infra). The formation of $H_{ox}(2)$ is very slow and only becomes discernible in samples in which the reaction with O_2 was quenched at times longer than 35 s.

The percent absorption (32 ± 5%) attributed to $H_{ox}(1)$ formed in this manner is identical to the initial percentage (32 ± 6%) obtained for $H_{red}(1)$ (vide supra), supporting the assignment that $H_{ox}(1)$ is the oxidized form of $H_{red}(1)$. Moreover, the Mössbauer parameters for $H_{ox}(1)$ are practically identical to those reported for H_{ox} from *M. trichosporium* OB3b.[11] In that case, H_{ox} did not appear to exhibit $H_{ox}(2)$, although a minority species (≈4%) was reported for that enzyme which resembles $H_{ox}(2)$.

Mössbauer Kinetic Data. With the various spectral components, $H_{red}(1)$, $H_{red}(2)$, the ferric impurity, $H_{ox}(1)$, and $H_{ox}(2)$, identified and their spectroscopic properties at zero-field characterized, it is possible to analyze the time-dependent Mössbauer spectra to identify reaction intermediates and garner kinetic information. In addition to the above-mentioned spectral components, the time-dependent Mössbauer spectra displayed in Figure 4 clearly reveal two transient sharp quadrupole doublets, corresponding to two reaction intermediates. Detection of the first intermediate in the *M. capsulatus* (Bath) enzyme, a diiron(III) peroxo species, was communicated previously.[26] The second intermediate, designated Q, has been identified in both the *M. trichosporium* OB3b and *M. capsulatus* (Bath) systems.[26,28,29] Visual inspection of the time-dependent Mössbauer spectra reveals that the formation of the peroxo species precedes the formation of Q. Since the spectral characteristics of all the components are known, it is possible to deconvolute their time-dependent behavior into individual components, and in this manner the percent absorption for each component as a function of time was accurately determined (Figure 7). The results clearly reveal the sequence of events occurring after reaction of $H_{red}(1)$ with dioxygen, namely, formation of the peroxo species, followed by its conversion to Q, followed by generation of the final diferric center (eq 4). The data were therefore analyzed according to eqs 5–7, which assume three consecutive,

$$H_{red} \xrightarrow{k_1} H_{peroxo} \xrightarrow{k_2} Q \xrightarrow{k_3} H_{ox} \tag{4}$$

$$[H_{peroxo}](t) = \frac{A^0{}_1 k_I}{k_2 - k_I}[\exp(-k_1 t) - \exp(-k_2 t)] \tag{5}$$

$$[Q](t) = \frac{A^0{}_1 k_1 k_2}{k_2 - k_1}\left[\frac{1}{k_3 - k_1}\exp(-k_1 t) - \frac{1}{k_3 - k_2} \times \exp(-k_2 t) + \left(\frac{1}{k_3 - k_2} - \frac{1}{k_3 - k_1}\right)\exp(-k_3 t)\right] \tag{6}$$

$$[H_{ox}(1)](t) = A^0{}_1\left\{\frac{k_1 k_2 k_3}{k_2 - k_1}\left[-\frac{\exp(-k_1 t)}{k_1(k_3 - k_1)} + \frac{\exp(-k_2 t)}{k_2(k_3 - k_2)} - \frac{\exp(-k_3 t)}{k_3}\left(\frac{1}{k_3 - k_2} - \frac{1}{k_3 - k_1}\right)\right] + 1\right\} \tag{7}$$

irreversible processes with rate constants k_1, k_2, and k_3, respectively. The least-squares fits of the data according to eqs 5–7 are plotted in Figure 7 and the derived rate constants are $k_1 = 28 \pm 5\ s^{-1}$, $k_2 = 0.4 \pm 0.15\ s^{-1}$, and $k_3 = 0.03 \pm 0.02\ s^{-1}$. This analysis also yielded a value of 32 ± 6% for the initial percentage of $H_{red}(1)$, which is identical to that obtained from the analysis of the decay of the diferrous components presented above. Also, the rate constant of 28 ± 5 s^{-1} determined for k_1 is consistent with the decay rate constant of 24 ± 5 s^{-1} determined for $H_{red}(1)$, providing additional evidence to support the notion that $H_{red}(1)$ is the precursor of H_{peroxo}. The good agreement observed between the experimental data and the fits justifies the proposed sequence of events described in eq 4. In other words, the Mössbauer kinetic data establish that the reaction of dioxygen with $H_{red}(1)$ forms first a peroxo intermediate which then decays to form the second intermediate, Q. The decay of Q generates the final product, $H_{ox}(1)$.

Mössbauer Spectroscopic Parameters of Intermediates. Table 3 summarizes the Mössbauer properties of the two transient intermediates. As shown in Figure 7, the amounts of H_{peroxo} and Q maximize at 156 ms and 8 s, respectively, after reaction of $H_{red}(1)$ with dioxygen. The zero-field Mössbauer spectra of the intermediates can be prepared from the raw spectra shown in Figure 4 (156 ms and 8 s spectra, respectively) by removing the contributions of other components. Such prepared spectra were previously communicated[26] and their characteristics may be summarized as follows. The 4.2 K zero-field Mössbauer

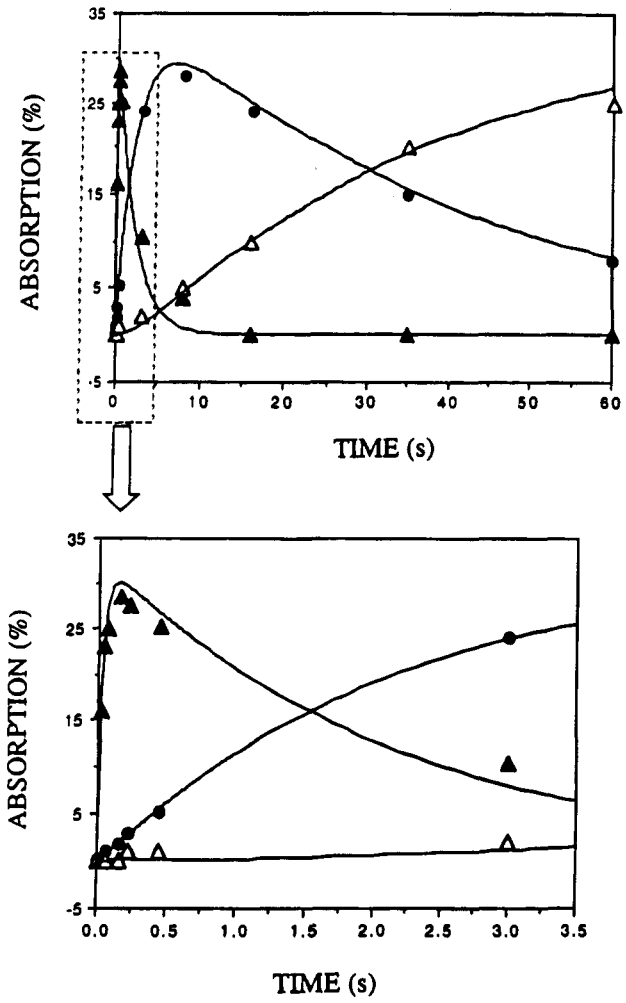

Figure 7. Time-dependent behavior of all species in the reaction of $H_{red}(1)$ with dioxygen at 4 °C, as monitored by Mössbauer spectroscopy. Solid triangles represent H_{peroxo}, solid circles represent intermediate Q, and open triangles represent H_{ox}. The upper figure shows the full 60 s time course, while the bottom is an expansion of the first 3.5 s of reaction time to demonstrate the buildup and decay of H_{peroxo}.

Table 3. Spectroscopic and Kinetic Parameters (at 4 °C) for Intermediates in the Reaction of H_{red} with Dioxygen

		M. capsulatus (Bath)[a]		*M. trichosporium* OB3b[b]
		H_{peroxo}	Q	Q
optical	λ_{max}, nm	≈625−650	350	330
			420	430
	k_{form},[c] s^{-1}	22	0.5	1
	k_{decay}, s^{-1}		0.07	0.05
Mössbauer (4K)	site 1:			
	δ, mm/s	0.66	0.21	0.17
	ΔE_Q, mm/s	1.51	0.68	0.53
	site 2:			
	δ, mm/s		0.14	
	ΔE_Q, mm/s		0.55	
	k_{form}, s^{-1}	28	0.4	
	k_{decay}, s^{-1}	0.4	0.03	
Raman	ν_{O-O}, cm^{-1}	905		

[a] See refs 26 and 27. [b] See refs 28 and 29. [c] $[O_2] \approx 1$ mM.

spectrum of the peroxo species is a sharp (line width = 0.27 mm/s) symmetric quadrupole doublet with $\Delta E_Q = 1.51 \pm 0.03$ mm/s and $\delta = 0.66 \pm 0.02$ mm/s. The spectrum of Q is a quadrupole doublet with a slightly broadened high-energy line which can be fit with two unresolved equal intensity quadrupole doublets ($\Delta E_Q = 0.68 \pm 0.03$ mm/s and $\delta = 0.21 \pm 0.02$ mm/s for doublet 1 and $\Delta E_Q = 0.55 \pm 0.03$ mm/s and $\delta = 0.14 \pm$ 0.02 mm/s for doublet 2). The corresponding spectrum of Q in the *M. trichosporium* OB3b system is symmetrical[28] and has parameters similar to the average values of the aforementioned two doublets. Spectra recorded at strong applied fields (4−8 T) reveal that both intermediates are diamagnetic (data not shown).

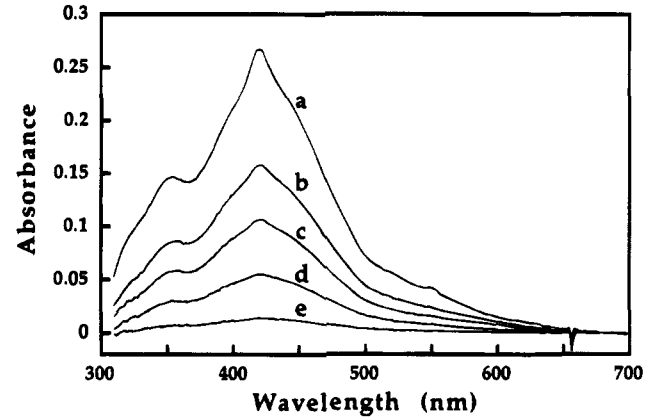

Figure 8. Decay of the optical spectrum of Q as monitored by stopped-flow spectroscopy at 4 °C. The time points depicted are (a) 6, (b) 11, (c) 15, (d) 35, and (e) 60 s. The λ_{max} values are 350, 420, and 520 (sh) nm.

Table 4. Activation Parameters from Arrhenius and Eyring Plots of the Reaction of H_{red} with Dioxygen

rate constant	E_a (kJ mol^{-1})	$\Delta H^{\ddagger}$ (kJ mol^{-1})	$\Delta S^{\ddagger}$ (J mol^{-1} K^{-1})
k_2	113	111	147
k_3	75	75	8

Optical Spectroscopic Characterization. Stopped-flow optical spectrophotometry at 4 °C was also used to analyze the kinetics of formation and decay of intermediate Q in the reactions of H_{red} with dioxygen in the presence of 2 equiv of protein B. As indicated in Figure 8, Q has two maxima at ≈350 and 420 nm which grow in and decay with time. Single wavelength absorption studies at 420 nm resulted in a well-defined kinetic trace (Figure S3), which was fit to the expression given in eq 8 describing two consecutive processes having rate constants of $k_2 \approx 0.5 \pm 0.15$ s^{-1} and $k_3 \approx 0.07 \pm 0.02$ s^{-1}. In the absence of protein B, the optical spectrum of Q could not be discerned.

$$y = [k_2A/(k_2 - k_3)][m(1 - \exp(-k_2t)) + n \exp(-k_3t)] \quad (8)$$

By using stopped-flow spectrophotometry, the kinetic constants k_2 and k_3 were derived under a variety of conditions. The results were unaffected by dioxygen concentration and were independent of pH in the range $6.6 \leq$ pH ≤ 8.6. When the reaction was run in D_2O with H_{red} that had previously been incubated in this solvent to exchange out protium for deuterium (see Experimental Section), there was little effect on the rate constants. The temperature dependence of the rate constants for formation and decay of Q was also measured. Arrhenius and Eyring plots of these data (Figure S4) yielded the parameters listed in Table 4.

The optical spectrum of Q was also recorded in the presence of substrate. With methane, high protein concentrations (>150 μM) were necessary to detect this intermediate. Fits of the observed kinetic traces revealed both k_2 and k_3 to increase slightly, to values of ≈0.95 and 0.17 s^{-1}, respectively. Analogous data were collected with the substrate hexane. The corresponding kinetic trace was fit with $k_3 \approx 0.13$ s^{-1}, but k_2 was unchanged. The optical spectrum of Q, taken in the

presence of either methane or hexane, revealed no new chromophore. Data obtained with nitrobenzene differ from those collected with methane and hexane since the product of the hydroxylation reaction, 4-nitrophenol, absorbs significantly at 400 nm. When monitored at 420 nm, k_2 was determined to be 0.26 s^{-1} and k_3, 0.11 s^{-1}. No other new optical bands were detected.

A summary of rate constants obtained from these studies is provided as supporting information (Table S1). Table 3 includes not only the Mössbauer but also the optical and resonance Raman spectral features of the two intermediates obtained from the present and related investigations of the reactions of H_{red} with dioxygen for proteins from both *M. capsulatus* (Bath)[26,27] and *M. trichosporium* OB3b.[28,29]

Discussion

sMMO Component Interactions as Assessed by Hydroxylation of Nitrobenzene. The interactions of protein B and reductase with the hydroxylase were evaluated by investigating the influence of these two components on the hydroxylation of nitrobenzene by H_{red}. Three aspects of this reaction were examined, the regioselectivity of hydroxylation, the overall product yield, and the rate constant for product formation. Analysis of the product alcohols indicated that hydroxylation of nitrobenzene proceeds in a regioselective manner depending on the reaction conditions. With chemically reduced hydroxylase, 4-nitrophenol was the predominant product irrespective of the amount of added protein B up to 4 equiv. Under catalytic conditions with all components, H_{ox}, protein B, reductase, and NADH, present, the distribution of products changed to an approximately equimolar mixture of 4-nitrophenol and 3-nitrophenol. The presence of reductase, therefore, altered the regioselectivity of hydroxylation to afford 3-nitrophenol, which was not produced by protein B and hydroxylase alone.

The product yield in single turnover reactions with H_{red} was also affected by the presence of the other components. Since HPLC analysis identified 4-nitrophenol as the predominant product under all conditions with H_{red}, the increased yields were not due to a shift in product distribution. Protein B markedly increased the yields. Addition of protein B and reductase to H_{red} resulted in diminished yields, however, and when added to H_{ox} prior to reduction, less than 5% hydroxylation was observed. Adding reductase alone to H_{ox} or H_{red} had very little effect on the yields relative to reactions with H_{red} alone. These results imply that protein B, and not the reductase, increases the yield of the hydroxylation reaction of nitrobenzene.

Protein B also increased the rate constant for single turnover reactions of H_{red} with nitrobenzene. Neither addition of reductase to H_{ox} or H_{red} nor addition of both protein B and reductase to H_{red} increased the rate constant relative to reactions of H_{red} alone. These observations again imply that protein B alone is sufficient to activate the hydroxylase and that protein B and reductase together do not significantly affect H_{red}. The pseudo-first-order rate constant for hydroxylation increased by up to 35-fold when H_{red} was treated with protein B (Figure 2). Complex formation among the three protein components of *M. trichosporium* OB3b sMMO has been demonstrated by use of chemical cross-linking agents and other methods.[23] It was hypothesized that protein B binds tightly to H_{ox} to form an activated complex, but then dissociates from H_{red} following electron transfer. The present results are consistent with initial binding of protein B to H_{ox} to form an activated complex following reduction. Because identical behavior was seen when protein B is added to H_{red}, we conclude that protein B can bind to H_{red} to form an activated complex as well. If the H_{red}–protein B complex is the species responsible for the increased rate constants, and H_{red} and protein B are in equilibrium between the complexed and uncomplexed forms, then the addition of more protein B would ensure that H_{red} is in the protein B-bound complex. Elevated concentrations of protein B beyond 2 equiv per H_{red} diminish the rate constant of the reaction (Figure 2), possibly by sterically hindering substrate binding to H_{red}. The total yield of reaction products could still remain high, since nearly all of the H_{red} is in the active, protein B-bound form. If there are adventitious binding sites for additional molecules of protein B beyond 2 equiv, excess protein B would have little effect once all such sites were fully occupied. This model is consistent with the B dependence of k_{obs} shown in Figure 2 and with the yields reported.

The present studies thus demonstrate that the reductase component of *M. capsulatus* (Bath) alters the product distributions of H_{red} with nitrobenzene but that protein B plays a more varied role in the sMMO system. In addition to helping regulate electron transfer from the reductase to the hydroxylase, protein B affects regioselectivity, k_{obs}, and product yields in single turnover reactions of H_{red}. Although a detailed molecular explanation for these observed functions remains a challenge for the future, the information was extremely valuable in helping to define conditions for the kinetic and spectroscopic experiments discussed below.

Intermediates in the Hydroxylase Reaction Cycle. Because optimal yields and rate constants in single turnover reactions were obtained in the presence of 2 equiv of protein B, these conditions were adopted for investigating the oxidation of H_{red} with dioxygen. Reactions were initially carried out in the absence of substrate in order to allow detectable concentrations of intermediates to accumulate, since these activated species were presumed to react quickly with substrate. The temperature was also lowered to 4 °C in order to slow the reaction and facilitate the detection of short-lived species.

Kinetic Studies by Mössbauer Spectroscopy. H_{red}, H_{ox}, and Protein Heterogeneity. Rapid freeze-quench Mössbauer spectroscopy was used to study the reaction of dioxygen with H_{red} from *M. capsulatus* (Bath). The results indicate that H_{red} contains at least two diferrous components that react differently with dioxygen. $H_{red}(1)$ reacts with a rate constant which is compatible with the known catalytic enzyme turnover rate, whereas $H_{red}(2)$ reacts with a slower rate constant that suggests catalytic incompetence. The relative amounts of $H_{red}(1)$ and $H_{red}(2)$ ranged from 1:2 to 2:3 over repeated sets of experiments. These ratios are consistent with the 40% maximum yield of nitrophenol in single turnover experiments, assuming that $H_{red}(2)$ does not hydroxylate substrate. There are several possible explanations for the presence of $H_{red}(2)$. One is that some of the enzyme might have been damaged either in vivo, prior to isolation and purification, or at some stage during these steps. Since the crystal structure of H_{ox} indicates the propensity of the core to bind exogenous ligands (Figure 1),[33] it is possible that $H_{red}(2)$ contains such a group, which could interfere with the reactivity of H_{red} toward dioxygen. Addition of acetate and other anions to the hydroxylase, however, has not yet been found to diminish its activity.[34,35] Alternatively, activity could depend on the Fe content of the enzyme. The hydroxylase has an $\alpha_2\beta_2\gamma_2$ composition, with the α subunit in each $\alpha\beta\gamma$ protomer housing a dinuclear iron core. Our typical preparations contain $\approx$2–3 mol of Fe per mole of protein instead of the theoretical value of 4, and it is possible that $H_{red}(2)$ is in some manner

(33) See discussions in refs 10 and 34.
(34) Rosenzweig, A. C.; Lippard, S. J. *Acc. Chem. Res.* **1994**, *27*, 229–236.
(35) Valentine, A. M.; Lippard, S. J. Unpublished results.

reflective of metal-depleted protomers. The large amount of $H_{ox}(2)$ present in sMMO from *M. capsulatus* (Bath) may account in part for the differences in specific activities previously reported for sMMO isolated from this organism[14,30] compared to the higher activity of protein obtained from *M. trichosporium* OB3b.[8] We are currently exploring alternative isolation techniques to determine what factors may alter the ratio of $H_{ox}(1)$ to $H_{ox}(2)$ in *M. capsulatus* (Bath).

To reflect the presence of the inactive $H_{red}(2)$ clusters, we can now adjust the extinction coefficients reported previously for intermediate Q[26] to $\epsilon_{350} \approx 3600$, $\epsilon_{420} \approx 7200$, and $\epsilon_{520} \approx 1400\ M^{-1}cm^{-1}$.

Mössbauer Characterization of Reaction Cycle Intermediates. Two diiron intermediates were detected for the reaction of dioxygen with $H_{red}(1)$ to generate the product diferric cluster $H_{ox}(1)$. Analysis of the kinetic data obtained from the Mössbauer measurements establishes that $H_{red}(1)$ reacts with dioxygen to form the first intermediate ($k_1 \approx 28\ s^{-1}$), which then decays irreversibly to form the second ($k_2 \approx 0.4\ s^{-1}$). In the absence of substrate, the latter decays slowly ($\approx 0.03\ s^{-1}$) to form $H_{ox}(1)$. In an earlier kinetic study of the reaction of dioxygen with H_{red} from *M. trichosporium* OB3b, the rate constant for the decay of H_{red}, as monitored by the disappearance of the $g = 16$ EPR signal, was $22 \pm 5\ s^{-1}$, whereas the rate constant for the formation of the second intermediate, designated Q, monitored by optical absorption at 430 nm, was $1\ s^{-1}$.[29] Based on these observations, an intermediate termed P was proposed to form at some point following the decay of H_{red} but prior to the generation of Q. Our results with the *M. capsulatus* (Bath) enzyme reveal that the hydroxylase from this organism reacts similarly with dioxygen. Furthermore, the kinetic data strongly suggest that the first intermediate, observed spectroscopically by us,[26,27] is equivalent to the proposed species P. In the *M. trichosporium* OB3b work, however, P was described as the immediate precursor to Q, but to leave room for other possible intermediates before Q, we introduced the letter L to describe this species.[26] Since L has now been identified as a diferric peroxo species (see below), we now refer to it as such rather than as L.[27]

The order of magnitude difference in the formation and decay rate constants of the two intermediates has made it possible to convert almost 100% of $H_{red}(1)$ to these species, facilitating their spectral characterization. Both exhibit Mössbauer parameters which are unusual for carboxylate-bridged diiron clusters. Based on chemical considerations, the kinetic data, and a recent resonance Raman study reporting an oxygen-isotope sensitive band at 905 cm^{-1},[27] we assign the first intermediate as a diiron(III) peroxide complex. Its observed isomer shift of 0.66 mm/s, however, is significantly outside the range of 0.52–0.54 mm/s reported for the few known diiron(III) peroxide complexes.[36–38] The larger isomer shift for H_{peroxo} was previously suggested to reflect a high iron coordination number and peroxide-to-iron charge transfer character,[26] and an isomer shift of 0.67 mm/s has been reported for a ferric peroxide heme model complex having these properties.[39]

The ligand environments of the few known diiron(III) peroxide model complexes are rich in nitrogen, whereas that of the hydroxylase comprises mostly oxygen ligands.[10,34] Although there is insufficient information to predict the effect of oxygen versus nitrogen ligation on the isomer shift of diiron(III) peroxo complexes, if the trend in ^{113}Cd NMR chemical shifts[40] can be extended to iron Mössbauer parameters, the order could be δ(oxygen) > δ(nitrogen) > δ(sulfur). The larger isomer shift may then reflect the oxygen-rich nature of the peroxo intermediate, as recently observed for an Fe(III)–EDTA peroxide complex which exhibits an isomer shift of 0.65 mm/s.[41] The sharp and symmetric Mössbauer spectrum[26] strongly suggests that the two iron sites in the intermediate are equivalent. This information, together with the recently available structural information on H_{red},[10b] leads us to assign the geometry as one of the symmetrical, bridged species presented in Figure 9.

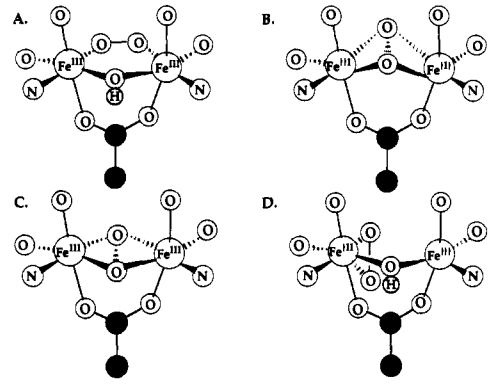

Figure 9. Possible structures for H_{peroxo}. We do not show η^1-peroxo structures, but cannot completely rule them out (see ref 27).

For structurally similar Fe complexes, the isomer shift is a good measure of oxidation state, following the trend $\delta_{Fe(II)} > \delta_{Fe(III)} > \delta_{Fe(IV)}$. The difference in isomer shift for each oxidizing equivalent is 0.4–0.5 mm/s.[42,43] Thus, one possibility is that the decrease in δ from 0.66 to 0.18 mm/s represents the expected change from the ferric state in the diiron(III) peroxide first intermediate to a formal diiron(IV) oxidation state in Q. Based on the observed diamagnetism and small isomer shift, intermediate Q of the hydroxylase from *M. trichosporium* OB3b was previously assigned to such a diiron(IV) state.[28] Although small, the observed isomer shift is greater than those reported for known heme and non-heme Fe(IV) complexes, however.[43–46] Moreover, we have thus far been unable to observe a resonance Raman band corresponding to a $Fe^{IV}{=}O$ stretching mode in freeze-quench samples of intermediate Q from *M. capsulatus* (Bath).[47] In a spectroscopic study of the assembly of the tyrosyl radical/(μ-oxo)diiron(III) center in the R2 subunit of *E. coli* ribonucleotide reductase, an intermediate was identified and tentatively assigned as a diiron(III)-radical species.[32] In the Mössbauer spectrum of this species, the two Fe(III) sites are inequivalent, with one iron site exhibiting an isomer shift (0.36 mm/s) significantly smaller than that of the other (0.55 mm/s). This reduction in isomer shift was proposed to be due to

(36) Brennan, B. A.; Chen, Q.; Juarez-Garcia, C.; True, A. E.; O'Connor, C. J.; Que, L., Jr. *Inorg. Chem.* **1991**, *30*, 1937–1943.
(37) Menage, S.; Brennan, B. A.; Juarez-Garcia, C.; Münck, E.; Que, L., Jr. *J. Am. Chem. Soc.* **1990**, *112*, 6423–6425.
(38) Micklitz, W.; Bott, S. G.; Bentsen, J. G.; Lippard, S. J. *J. Am. Chem. Soc.* **1989**, *111*, 372–374.
(39) Burstyn, J. N.; Roe, J. A.; Miksztal, A. R.; Shaevitz, B. A.; Lang, G.; Valentine, J. S. *J. Am. Chem. Soc.* **1988**, *110*, 1382–1388.
(40) Vogel, H. J., Forsén, S. In *Biological Magnetic Resonance*; Berliner, L. J., Reuben, J., Eds.; Plenum Press: New York, 1987; pp 249–309.
(41) Münck, E. Personal communication.
(42) Christou, G.; Mascharak, P. K.; Armstrong, W. H.; Papaefthymiou, G. C.; Frankel, R. B.; Holm, R. H. *J. Am. Chem. Soc.* **1982**, *104*, 2820–2831.
(43) *Iron Porphyrins*; Debrunner, P. G., Ed.; VCH Publishers: New York, 1990; pp 139–234.
(44) Collins, T. J.; Kostka, K. L.; Münck, E.; Uffelman, E. S. *J. Am. Chem. Soc.* **1990**, *112*, 5637–5639.
(45) Kostka, K. L.; Fox, B. G.; Hendrich, M. P.; Collins, T. J.; Rickard, C. E. F.; Wright, L. J.; Münck, E. *J. Am. Chem. Soc.* **1993**, *115*, 6746–6757.
(46) Vogel, E.; Will, S.; Tilling, A. S.; Neumann, L.; Lex, J.; Bill, E.; Trautwein, A. X.; Wieghardt, K. *Angew. Chem., Int. Ed. Engl.* **1994**, *33*, 731–735.
(47) Valentine, A. M.; Liu, K. E.; Qiu, D.; Edmondson, D. E.; Spiro, T. G.; Lippard, S. J. Unpublished results.

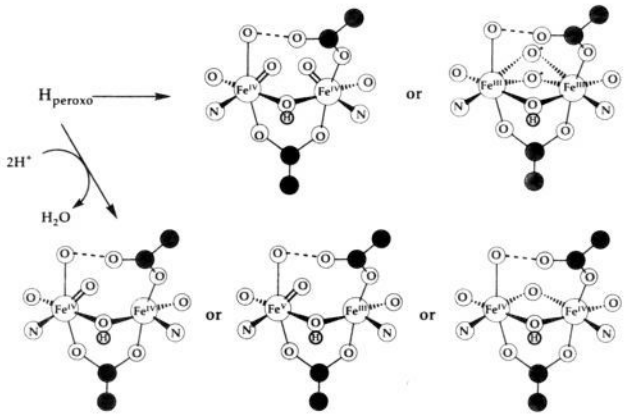

Figure 10. Possible structures for intermediate Q.

coordination of the radical, which has a strong tendency to withdraw electron density from its environment. Similar arguments may apply here to explain the small δ value of Q. Figure 10 illustrates possible structures for intermediate Q, which represent various manifestations of these two classes. Included are $Fe^{IV}{=}O$ and $Fe^{III}{-}O^{\bullet -}$ species, which can be formed by a homolytic cleavage of the O−O bond in H_{peroxo}. The inequivalence of the Fe sites observed in the Mössbauer data (Figure 4, Table 2) could reflect significant rearrangement of the protein ligands, e.g. carboxylate shifts, in Q as compared to H_{peroxo} and H_{ox}. Alternatively, the oxygen atom of the proposed Fe(IV) oxo or Fe(III) oxyl radical species may not be bound symmetrically between the Fe atoms. Protonation and heterolytic cleavage of the O−O bond, as proposed for cytochrome P-450,[48] could similarly lead to $Fe^{IV}{=}O$ or $Fe^{III}{=}O^{\bullet -}$ units (Figure 10).

Among the known diiron model complexes there exists a bis(μ-oxo) species[49] which exhibits Mössbauer parameters very similar to those observed for intermediate Q. Initially, this complex was assigned as a mononuclear Fe(IV)−oxo radical complex.[49] It was largely on the basis of this assignment that the isomer shift of 0.12 mm/s for the complex was used as a justification for the diiron(IV) assignment for Q.[28] More detailed characterization subsequently revealed the complex to *be a* $\{Fe_2(\mu\text{-}O)_2\}^{3+}$ *unit with a mixed-valent Fe(III)−Fe(IV)* formal oxidation state.[50] The similarity between the Mössbauer parameters of Q and that of the model can therefore no longer be used as a justification for assigning a diiron(IV) state for the protein intermediate. In particular, there are major differences between the properties of this complex and those of Q. First, the oxidation states are different; Q is 1 equiv more oxidized than the bis(μ-oxo) complex. Second, the iron coordination of the bis(μ-oxo) complex is N_4O_2 whereas only a single nitrogen donor ligand per Fe site is available for Q. Finally, the spin states differ since the complex has a ground state of $^3/_2$ whereas Q is diamagnetic. Nevertheless, this bis(μ-oxo) complex, formed as an intermediate in the reaction of H_2O_2 with a (μ-oxo)(μ-hydroxo)diiron(III) precursor,[50] offers some insights into the nature of Q. If we assume on the basis of their similar isomer shifts that the bis(μ-oxo) model complex and Q have similar +3.5 iron oxidation states, and since Q has one fewer electron than the model, it may be that the electron is removed from a ligand or an active site residue and not from the iron atoms. An antiferromagnetically coupled $RS^{\bullet}/Fe^{III}{}_2(O^{\bullet -})$ diradical species suggested previously[4] is one possibility.

Optical Spectroscopic Kinetic Studies. As indicated in Figure 8, intermediate Q has several intense electronic spectral bands not previously observed in non-heme diiron model complexes. The absorptions might be high spin ferric d−d transitions, intensity-enhanced in a manner similar to those in known (μ-oxo)diiron(III) complexes,[51] but more work is required to obtain a definitive assignment. Stopped-flow kinetic studies with optical detection at 420 nm yielded rate constants for the growth and decay of Q that were fit cleanly to a biexponential equation with a single growth and a single decay phase. These rate constants derived from fits to eq 6 match within experimental error those determined from the kinetic Mössbauer data (Tables 3 and S1).

Conversion of the diiron(III) peroxide intermediate into any of the species proposed above for Q requires cleavage of the O−O bond and release of a water molecule. From the temperature dependence of the rate constant for conversion of H_{peroxo} to Q, we calculated a large $\Delta S^{\ddagger}$ value of 147 ± 5 J mol^{-1} K^{-1}. This result requires a transition state having increased degrees of freedom, which is consistent with O−O bond cleavage and possibly release of a water molecule. The corresponding $\Delta S^{\ddagger}$ value of 8 ± 0.5 J mol^{-1} K^{-1} for the decay of Q is considerably smaller. At present we do not know the fate of the oxygen atom that would ordinarily be transferred to substrate, so it is difficult to interpret this kinetic parameter. The $\Delta H^{\ddagger}$ values in Table 4 imply significant bond rearrangement during both of these transition states.

The rate constants obtained both for the formation and the decay of Q were independent of the concentration of dioxygen. This observation is consistent with H_{peroxo} being formed irreversibly in the reaction of H_{red} with dioxygen. The rate constant for H_{peroxo} formation is expected to have a first-order dependence on the concentration of dioxygen in the system. Study of this reaction by stopped-flow techniques has proved to be more difficult, owing to its lower extinction coefficient and shorter lifetime. Preliminary results revealed a peroxo-to-iron charge transfer band with $\lambda_{max} \approx 600{-}650$ nm ($\epsilon \approx 1500$ M^{-1}cm^{-1}) which appeared with $k \approx 20$ s^{-1}.[27] Further studies of this reaction are in progress. If formation of H_{peroxo} is irreversible, and since it proceeds with a rate constant ($\approx$25 s^{-1}) which is nearly two orders of magnitude greater than the rate constant for Q formation ($\approx$0.4 s^{-1}), the latter should only be dioxygen-dependent at very low O_2 concentrations. Lack of dioxygen dependence as measured through intermediate Q formation is therefore consistent with a mechanism in which H_{red} reacts irreversibly with dioxygen to produce H_{peroxo} which then decays more slowly to form Q.

Since the reaction catalyzed by the sMMO system requires two protons, the consequences of altering the pH and of replacing the exchangeable protons by deuterons on the kinetic behavior of Q formation and decay were investigated. Except for an increase in k_3 to a value of $\approx$0.145 s^{-1} in the deuterated enzyme, no differences were observed. This finding does not address the issue of whether or not proton transfer occurs in either of these steps, but does indicate that proton transfer is not rate determining. If proton transfer were rate determining in the formation or decay of Q, a significant decrease in k_2 or k_3 might be expected. This result is consistent with O−O bond cleavage as the rate determining step in Q formation (Figure 10).

(48) Ortiz de Montellano, P. R. In *Cytochrome P-450 Structure, Mechanism, and Biochemistry*; Ortiz de Montellano, P. R., Ed.; Plenum Publishing Corp.: New York, 1986; pp 217−271.

(49) Leising, R. A.; Brennan, B. A.; Que, L., Jr.; Fox, B. G.; Münck, E. *J. Am. Chem. Soc.* **1991**, *113*, 3988−3990.

(50) Dong, Y.; Fujii, H.; Hendrich, M. P.; Leising, R. A.; Pan, G.; Randall, C. R.; Wilkinson, E. C.; Zang, Y.; Que, L., Jr.; Fox, B. G.; Kauffmann, K.; Münck, E. *J. Am Chem. Soc.* **1995**, *117*, 2778−2792.

(51) Brown, C. A.; Remar, G. J.; Musselman, R. L.; Solomon, E. I. *Inorg. Chem.* **1995**, *34*, 688−717.

In the presence of methane, hexane, and nitrobenzene, much less Q accumulated when compared to reactions run in the absence of a hydrocarbon substrate. This result indicated that Q is a kinetically competent intermediate in the hydroxylation mechanism. In all cases k_3 increased. Although no additional optical bands were detected following the decay of Q, the substrates are assumed to react with this species. With methane, Q was observed only at high concentrations of H_{red}, and k_2 also increased slightly. The ability of methane to affect the rate constant for Q formation is unexpected. A possible explanation for this behavior is that this substrate alters the environment of the active site, for example by making it more hydrophobic and promoting the release of a water molecule. Such behavior could favor the conversion of H_{peroxo} to Q in some of the possible mechanisms discussed earlier. With both hexane and nitrobenzene, k_2 was not affected significantly, implying that these substrates had little effect on the conversion of H_{peroxo} to Q.

Comparisons with Analogous Studies of sMMO from *M. trichosporium* OB3b. Component Interactions. Table 1 compares the present results for catalytic oxidation of nitrobenzene with those obtained in analogous studies with sMMO from *M. trichosporium* OB3b.[25] In this system, unlike that from *M. capsulatus* (Bath), protein B is apparently not required to sustain turnover under catalytic conditions,[8] and H_2O_2 can support high levels of turnover in a shunt pathway with H_{ox} alone.[24,25,52] This peroxide shunt affords lower levels of oxidation in *M. capsulatus* (Bath).[53] Investigation of the regioselectivity of nitrobenzene hydroxylation with the *M. trichosporium* OB3b enzyme[25] revealed that ≥90% of the product is 3-nitrophenol under catalytic conditions without protein B. Adding 0.1 to 2 equiv of protein B to hydroxylase, reductase, and NADH afforded 83−89% of 4-nitrophenol. In this case, therefore, protein B shifts the product distribution toward 4-nitrophenol. In the H_2O_2 shunt pathway of H_{ox} from *M. trichosporium* OB3b,[24] almost equal amounts of 4-nitrophenol and 3-nitrophenol were produced, which matches behavior seen with the catalytic system from *M. capsulatus* (Bath). It is also noteworthy that the K_M (≈5 mM) for nitrobenzene with the catalytic sMMO system from *M. capsulatus* (Bath) matches the K_M value of H_{ox} and H_2O_2, but not the K_M value (≈100 μM) for the catalytic system from *M. trichosporium* OB3b. From these results and the data in Table 1, it is apparent that the component interactions in the two systems are complex and alter the hydroxylation chemistry in different manners.

As described above, a 35-fold increase in the rate constant for hydroxylation occurred when protein B was added during single turnover reactions. This behavior parallels that reported for protein B from *M. trichosporium* OB3b for titrations performed with H_{ox} and reductase under catalytic turnover conditions.[23] In contrast to the present single turnover reactions of nitrobenzene with H_{red} from *M. capsulatus* (Bath), protein B had little effect on the rates of analogous reactions of H_{red} from *M. trichosporium* OB3b.[25] Instead, protein B from *M. trichosporium* OB3b increased the initial velocity of the complete reconstituted system (H_{ox}, reductase, NADH, catalytic conditions), but decreased initial velocities in reactions of H_{ox} with H_2O_2. Thus, as with the product distribution studies, component interactions affect the kinetic behavior differently for the two sMMO systems. More structural work on component interactions with both sMMO systems is essential to understand fully the reasons for the observed effects on the rate constants and yields of the reactions.

Intermediates. The similar spectroscopic properties and kinetic rate constants observed for the formation and decay of intermediates in the reaction cycle of the hydroxylases from *M. capsulatus* (Bath) and *M. trichosporium* OB3b reveal that, despite the above delineated nuances in product distribution and previous subtle differences observed by using radical clock substrate probes,[30] the two sMMO systems have closely related reaction mechanisms. This result is remarkable, given the divergent evolutionary histories of the two organisms.[54]

In studies with *M. trichosporium* OB3b, the growth and decay of Q were best fit to a triexponential equation, which included two separate growth curve components.[29] The origin of these separate processes was attributed to discrete H_{red}/B complexes that react with dioxygen with different rate constants to form Q, behavior which was not observed in the *M. capsulatus* (Bath) system. The average rate constant for growth, $1 \pm 0.1\ s^{-1}$, was about twice the value reported here for *M. capsulatus* (Bath), but both sMMO systems had similar decay constants of ≈ 0.05 and $0.065\ s^{-1}$. The optical spectrum of an unexplained species that formed but did not further react was observed in the reaction with *M. trichosporium* OB3b, and was subtracted from the observed spectrum to reveal that of Q.[29] This species may arise from $H_{red}(2)$, as observed with *M. capsulatus* (Bath), but $H_{red}(2)$ from *M. trichosporium* OB3b may be present in smaller quantities, rendering undetectable its even spin EPR signal and Mössbauer spectrum.

Differences between the chemistry of the two sMMO systems that do occur probably evolve in the reaction of Q with substrates. For example, we did not see any evidence for binding of the hydroxylation product of nitrobenzene to H_{ox} in a single turnover reaction, whereas hydroxylation of nitrobenzene in the *M. trichosporium* OB3b system afforded an intermediate designated T.[29] This intermediate was observed only with nitrobenzene, and gave rise to an optical band at 430 nm assigned to the bound product phenol. Such a difference may reflect the different binding affinities of the product to the active site in the two systems, which could be attenuated by differences in protein B binding.

Summary and Conclusions

Single turnover reactions of H_{red} with nitrobenzene are highly dependent on the concentration of protein B in the system. Both the yield and rate constant of the reaction are optimized at a 1.5−2:1 ratio of B:H. The regioselectivity of the reaction under these conditions differs substantially from reactions performed under catalytic conditions with all components present, where the reductase plays a key role. By lowering the temperature and omitting substrate from the above reactions, two intermediates along the reaction pathway were identified and kinetically characterized. Structures consistent with the Mössbauer, optical, and resonance Raman spectroscopic characterization of these intermediates were proposed. The unusual Mössbauer parameters for these intermediates will require the synthesis of appropriate model complexes.

From the present and related results, we propose the catalytic hydroxylation cycle for sMMO from *M. capsulatus* (Bath) illustrated in Figure 11. The reaction begins with the resting state of the enzyme, H_{ox}. Binding of substrate and subsequent electron transfer through the reductase yields the H_{red}−substrate complex. Dioxygen next reacts with H_{red} and forms H_{peroxo}. This species then evolves a second intermediate, Q, of uncertain

(52) Froland, W. A.; Andersson, K. K.; Lee, S.-K.; Liu, Y.; Lipscomb, J. D. In *IUCCP Symposium on Applications of Enzyme Biotechnology*; Plenum Press: College Station, TX, 1991; pp 39−54.

(53) Jiang, Y.; Wilkins, P. C.; Dalton, H. *Biochim. Biophys. Acta* **1993**, *1163*, 105−112.

(54) Bowman, J. P.; Sly, L. I.; Nichols, P. D.; Hayward, A. C. *Int. J. Syst. Bacteriol.* **1993**, *43*, 735−753.

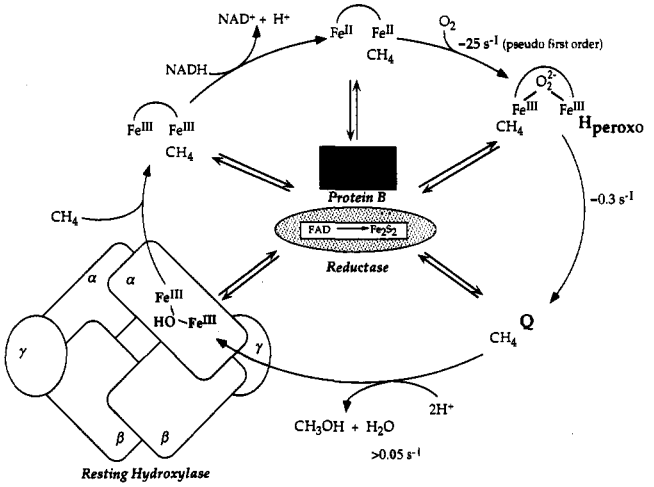

Figure 11. Summary of the known features of the catalytic cycle of sMMO from *M. capsulatus* (Bath).

composition and structure, which then reacts with substrate. It is not known whether proton transfer accompanies the O–O bond cleaving step or whether Fe–C bond formation might occur. Product dissociation regenerates H_{ox}, and the cycle is ready to begin again. Rate constants for each step are as indicated in the figure, and the available activation parameters are consistent with this proposal.

Acknowledgment. This work was supported by grants from the National Institute of General Medical Science (GM32134 to S.J.L., GM47295 to B.H.H., and GM29433 to D.E.E.), the National Science Foundation (DMB9001530 to B.H.H.), and Shell (S.J.L.). We thank Dr. Axel Masschelein for advice and experimental assistance, Andrew Feig for helpful discussions, and Dr. Sonja Komar-Panicucci for help in preparing Figure 11.

Supporting Information Available: Details of the HPLC characterization of products from single turnover reactions, a tabulation of rate constants under various conditions (Table S1), the effect of protein B on single turnover yields with nitrobenzene (Figure S1), the evolution of 4-nitrophenol under single turnover conditions in the absence and presence of B (Figure S2), the optical trace of intermediate Q with and without protein B (Figure S3), Arrhenius and Eyring plots for the formation and decay of Q (Figure S4), and the optical signal for Q in the presence of methane (Figure S5) (7 pages). This material is contained in many libraries on microfiche, immediately follows this article in the microfilm version of this journal, can be ordered from the ACS, and can be downloaded from the Internet; see any current masthead page for ordering information and Internet access instructions.

JA951836I